5 Introduction to Dynamical Mean-Field Theory

Marcus Kollar
Center for Electronic Correlations and Magnetism
University of Augsburg

Contents

1 Introduction **2**

2 Fermions in infinite dimensions **6**

3 Simplifications for many-body theory **9**

4 Dynamical mean-field theory **12**

5 Summary and outlook **17**

Eva Pavarini, Erik Koch, Dieter Vollhardt, and Alexander Lichtenstein (eds.)
The LDA+DMFT approach to strongly correlated materials
Forschungszentrum Jülich 2011, ISBN 978-3-89336-734-4

1 Introduction

The previous lectures have already discussed several aspects of the physics of correlated electrons in solids, i.e., electrons for which the Coulomb interaction is important and whose behavior cannot be assumed to be independent of one another. Several ingredients are necessary to successfully describe such correlated materials: the Hamiltonian describing the electronic physics must be obtained, both the interaction part and the kinetic part (i.e., the band structure as determined with density functional theory, which also provides a suitable basis). Then the interaction must be treated reliably, and for this dynamical mean-field theory (DMFT) and related theories provide a controlled approach. The spirit and some technical aspects of DMFT were already mentioned in the Lecture of D. Vollhardt. The purpose of the present chapter is to provide a derivation of DMFT (one of many possible derivations, see, e.g., Ref. [1–3]), which becomes exact in the limit of infinite spatial dimensions.
We assume that the band structure and interaction are known, leading to a one- and two-body Hamiltonian of the type

$$H = \sum_{ij\alpha\beta\sigma} t_{ij}^{\alpha\beta}\; c_{i\alpha\sigma}^{+} c_{j\beta\sigma} \quad + \frac{1}{2} \sum_{\substack{ijkl \\ \alpha\beta\gamma\delta\sigma\sigma'}} V_{ijkl}^{\alpha\beta\gamma\delta}\; c_{i\alpha\sigma}^{+} c_{j\beta\sigma'}^{+} c_{l\delta\sigma'} c_{k\gamma\sigma}\,. \tag{1}$$

For the present purpose we assume that this Hamiltonian can be reduced further: we keep only a single band and only the on-site Hubbard interaction $U = V_{iiii}$, leading to the single-band Hubbard model:

$$H = H_0 + H_1\,, \qquad H_1 = U \sum_i n_{i\uparrow} n_{i\downarrow}\,, \tag{2a}$$

$$H_0 = \sum_{ij\sigma} t_{ij}\; c_{i\sigma}^{+} c_{j\sigma} = \sum_{\boldsymbol{k}\sigma} \epsilon_{\boldsymbol{k}}\; c_{\boldsymbol{k}\sigma}^{+} c_{\boldsymbol{k}\sigma}\,, \tag{2b}$$

where t_{ij} is the hopping amplitude from site i to j, whose Fourier transform is the dispersion relation $\epsilon_{\boldsymbol{k}}$.
We begin by reviewing some definitions and basic concepts of many-body physics that are useful for the formulation and application of DMFT. In Sec. 2 we consider the limit of infinite dimensions and analyze what happens to the kinetic Hamiltonian H_0 in this limit; in particular the hopping matrix elements must be scaled correctly with the diverging lattice dimension. In Sec. 3 we discuss what happens to the many-body perturbation series as a consequence of this scaling, i.e., that the self-energy becomes local. Finally, it is shown how this local self-energy can actually be calculated in DMFT (Sec. 4).

Green functions

An important dynamical quantity which measures the equilibrium properties of a correlated electron system is the electronic Green function [4,5]. In general a Green function G_{AB} is defined as an expectation value of operators A and B taken at different (real or imaginary) times

in a thermal state, i.e., with density matrix $\propto \exp(-\beta(H-\mu N))$ corresponding to the temperature $T = 1/\beta$, or possibly the ground state. Hence it measures the probability amplitude for a propagation of a particle or hole excitation in an equilibrium state if A and B are annihilation and creation operators.

In finite-temperature problems one often uses the imaginary-time-ordered (fermionic) single particle Green function $G_{\alpha\beta}(\tau)$ (we put $A = c_\alpha\,, B = c_\beta^+$):[1]

$$G_{\alpha\beta}(\tau) = -\langle T_\tau c_\alpha(\tau) c_\beta^+(0)\rangle = -\begin{cases} \langle c_\alpha(\tau) c_\beta^+(0)\rangle & \tau > 0 \\ -\langle c_\beta^+(0) c_\alpha(\tau)\rangle & \tau \le 0 \end{cases} \tag{3}$$

$$= -G_{\alpha\beta}(\tau+\beta) \quad \text{for } -\beta < \tau < 0, \tag{4}$$

with imaginary-time Heisenberg operators $A(\tau) = e^{H\tau} A e^{-H\tau}$; note that $A^+(\tau) \neq A(\tau)^+$. Its dependence on time difference only and the anti-periodicity (4) follow from the cyclic properties of the trace. A Fourier transform yields the Matsubara Green function $G_{\alpha\beta}(i\omega_n)$:

$$G_{\alpha\beta}(i\omega_n) = \int_0^\beta d\tau\; G_{\alpha\beta}(\tau)\; e^{i\omega_n\tau}\,, \qquad G_{\alpha\beta}(\tau) = T\sum_{n=-\infty}^{+\infty} G_{\alpha\beta}(i\omega_n)\; e^{-i\omega_n\tau}\,, \tag{5}$$

with fermionic Matsubara frequencies $i\omega_n = 2\pi T(n+\frac{1}{2})$. It is useful to note the spectral representation

$$G_{\alpha\beta}(i\omega_n) = \int_{-\infty}^{\infty} d\omega \frac{A_{\alpha\beta}(\omega)}{i\omega_n - \omega}, \tag{6}$$

with the spectral function given by its Lehmann representation as (Z: partition function, E_n: eigenvalues of $H-\mu N$)

$$A_{\alpha\beta}(\omega) = \frac{1}{Z}\sum_{n,m} \langle n|c_\beta^+|m\rangle\langle m|c_\alpha|n\rangle\; (e^{-\beta E_m} - e^{-\beta E_n})\; \delta(\omega - (E_n - E_m))\,. \tag{7}$$

In particular $A_{\alpha\alpha}(\omega) \geq 0$. Note that in practice the spectral or Green function can be evaluated via the Lehmann representation only for sufficiently small systems, i.e., when the many-body energy eigenvalues and eigenstates can be obtained directly.

From the spectral function other single-particle Green functions can also be obtained, such as the retarded Green function

$$G^{\text{ret}}_{\alpha\beta}(\omega) = \int_{-\infty}^{\infty} d\omega' \frac{A_{\alpha\beta}(\omega')}{\omega + i0^+ - \omega'}\,, \tag{8}$$

which corresponds to a Green function in the time domain that involves real-time Heisenberg operators. We note that

$$A_{\alpha\beta}(\omega) = -\frac{1}{\pi}\text{Im}\, G^{\text{ret}}_{\alpha\beta}(\omega)\,, \tag{9}$$

[1] Note that the prefactor -1 is omitted from the definition in Ref. [5].

and that the retarded Green function can be obtained from the Matsubara Green function by the analytic continuation from $i\omega_n$ to $\omega + i0^+$. In view of the spectral representations (6) and (8) we will often write $G_{\alpha\beta}(\omega)$ for both the Matsubara or retarded Green function, with the understanding that the argument is either $i\omega_n$ for the former and $\omega + i0^+$ for the latter (and hence is never purely real).
The indices $\alpha, \beta, \ldots$ can represent lattice site or momentum $\boldsymbol{k}$, as well as spin index σ (and possibly orbital or band index). The real-space and momentum-space Green functions are related by a Fourier transform. We will work in particular with the local Green function (L: number of lattice sites)

$$G_{ii\sigma}(\omega) = G_\sigma(\omega) = \frac{1}{L}\sum_{\boldsymbol{k}} G_{\boldsymbol{k}\sigma}(\omega)\,, \qquad A_{ii\sigma}(\omega) = A_\sigma(\omega) = -\frac{1}{\pi}\mathrm{Im}\; G_\sigma(\omega + i0^+)\,, \tag{10}$$

assuming translational invariance.
Free particles, with Hamiltonian $H - \mu N = \sum_{\boldsymbol{k}\sigma}(\epsilon_{\boldsymbol{k}} - \mu)\; c^+_{\boldsymbol{k}\sigma} c_{\boldsymbol{k}\sigma}$, are characterized by the free Green function $G^{(0)}_{\boldsymbol{k}\sigma}(\omega)$ and the free density of states $\rho(\epsilon)$,[2]

$$G^{(0)}_{\boldsymbol{k}\sigma}(\omega) = \frac{1}{\omega + \mu - \epsilon_{\boldsymbol{k}}}, \qquad \rho(\omega) = A^{(0)}_\sigma(\omega) = \frac{1}{L}\sum_{\boldsymbol{k}} \delta(\omega - \epsilon_{\boldsymbol{k}})\,. \tag{11}$$

For interacting systems the self-energy $\Sigma_{\boldsymbol{k}}(\omega)$ is defined so that it measures the difference between interacting and free Green functions:

$$G_{\boldsymbol{k}\sigma}(\omega)^{-1} = G^{(0)}_{\boldsymbol{k}\sigma}(\omega)^{-1} - \Sigma_{\boldsymbol{k}\sigma}(\omega)\,, \qquad G_{\boldsymbol{k}\sigma}(\omega) = \frac{1}{\omega + \mu - \epsilon_{\boldsymbol{k}} - \Sigma_{\boldsymbol{k}\sigma}(\omega)}\,. \tag{12}$$

For a translationally invariant system the Green function and self-energy are diagonal in momentum space. It can also be useful instead to use a matrix notation in site indices, $G_{ij\sigma}(i\omega_n) = (\boldsymbol{G})_{ij,\sigma,n}$ etc., for which

$$\boldsymbol{G}^{-1} = \boldsymbol{G}^{(0)\,-1} - \boldsymbol{\Sigma}\,, \qquad \boldsymbol{G} = \boldsymbol{G}^{(0)} + \boldsymbol{G}^{(0)}\boldsymbol{\Sigma}\boldsymbol{G}\,. \tag{13}$$

Eq. (12) or (13) are referred to as the (lattice) Dyson equation. The Dyson equation (in any basis) can be expressed with Feynman diagrams as

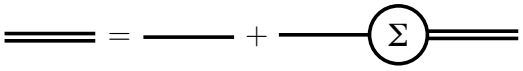

(14)

We will discuss Feynman diagrams for the self-energy in Sec. 3.

Path-integral formulation

Another useful technique to work with Green functions is the path integral representation [5]. The partition function and the imaginary-time-ordered Green function for the fermionic Hamil-

[2] In the thermodynamic limit ($L \to \infty$), the sum over the first Brillouin zone in (11) can be replaced by an integral, see e.g. (28) below.

tonian $H(\{c_\alpha^+\},\{c_\alpha\})$ can be written in terms of functional integrals over Grassmann variables,

$$Z = \mathrm{Tr} e^{-\beta(H-\mu N)} = \int\limits_{\phi_\alpha(\beta)=-\phi_\alpha(0)} \mathcal{D}(\phi_\alpha^*(\tau),\phi_\alpha(\tau))\ \exp(\mathcal{A}), \tag{15}$$

$$G_{\alpha\beta}(\tau) = \frac{1}{Z} \int\limits_{\phi_\alpha(\beta)=-\phi_\alpha(0)} \mathcal{D}(\phi^*\phi)\ \phi_\alpha(\tau)\phi_\beta^*(0)\ \exp(\mathcal{A}), \tag{16}$$

with the action

$$\mathcal{A} = -\int_0^\beta d\tau \left[\sum_\alpha \phi_\alpha^*\left(\partial_\tau - \mu\right)\phi_\alpha + H(\{\phi_\alpha^*\},\{\phi_\alpha\})\right]. \tag{17}$$

Note that the Grassmann fields $\phi_\alpha^*(\tau)$ and $\phi_\alpha(\tau)$ are independent (i.e., they are not complex or hermitian conjugates of each other, even though they represent creation and annihilation operators) and antiperiodic boundary conditions are imposed on the latter. Strictly speaking, path-integral expressions such as (16) and (17) are merely shorthand for limits of expressions that are discretized in imaginary time τ. We refer to Ref. [5] for details.

Quasiparticles

Without interactions single-particle excitations can be created and propagated freely. In a large many-body system with interactions, on the other hand, particle or hole excitations will usually be damped and have a finite lifetime. This is encoded in the complex (retarded) self-energy $\Sigma_{\boldsymbol{k}}(\omega)$, in terms of which the spectral function becomes

$$A_{\boldsymbol{k}}(\omega) = \frac{1}{\pi}\frac{\mathrm{Im}\Sigma_{\boldsymbol{k}}(\omega)}{(\omega+\mu-\epsilon_{\boldsymbol{k}}-\mathrm{Re}\Sigma_{\boldsymbol{k}}(\omega))^2+(\mathrm{Im}\Sigma_{\boldsymbol{k}}(\omega))^2}\,. \tag{18}$$

This reduces to a δ function only if $\mathrm{Im}\Sigma_{\boldsymbol{k}}(\omega)\to 0^-$. On the other hand, if $\mathrm{Im}\Sigma_{\boldsymbol{k}}(\omega)$ is finite and not too large, the maxima of $A_{\boldsymbol{k}}(\omega)$ are located approximately at the zeros $\omega = E_{\boldsymbol{k}}$ of

$$\omega+\mu-\epsilon_{\boldsymbol{k}}-\mathrm{Re}\Sigma_{\boldsymbol{k}}(\omega) = 0\,. \tag{19}$$

In the vicinity of $E_{\boldsymbol{k}}$ the Green function can then be approximated to lowest order as

$$G_{\boldsymbol{k}}(\omega) = \frac{Z_{\boldsymbol{k}}(E_{\boldsymbol{k}})}{\omega - E_{\boldsymbol{k}} + i\tau_{\boldsymbol{k}}(E_{\boldsymbol{k}})^{-1}}\,, \tag{20a}$$

$$Z_{\boldsymbol{k}}(\omega) = [1-\mathrm{Re}\Sigma_{\boldsymbol{k}}(\omega)]^{-1}\,, \tag{20b}$$

$$\tau_{\boldsymbol{k}}(\omega) = [-Z_{\boldsymbol{k}}(\omega)\mathrm{Im}\Sigma_{\boldsymbol{k}}(\omega)]^{-1}\,, \tag{20c}$$

where $Z_{\boldsymbol{k}}$ and $\tau_{\boldsymbol{k}}$ play the role of a quasiparticle weight and lifetime. In analogy to the non-interacting case the maxima $E_{\boldsymbol{k}}$ of $A_{\boldsymbol{k}}(\omega)$ yield the *electronic dispersion*, i.e., the relation between crystal momentum and excitation energy, although this maximum may be quite broad.

A reliable quasiparticle picture is guaranteed in a Landau Fermi liquid close to the Fermi surface, i.e., near $\omega = 0$, because then $\mathrm{Re}\Sigma_{\boldsymbol{k}}(\omega)$ is linear and $\mathrm{Im}\Sigma_{\boldsymbol{k}}(\omega)$ quadratic in ω for small frequencies. Near $\omega = 0$ this leads to

$$E_{\boldsymbol{k}} = Z_{\boldsymbol{k}}(0)(\epsilon_{\boldsymbol{k}} - \mu + \mathrm{Re}\Sigma_{\boldsymbol{k}}(0))\,, \tag{21}$$

i.e., a linear relation between bare and interacting dispersion. However angle-resolved photoemission (ARPES) nowadays provides a means to measure $A_{\boldsymbol{k}}(\omega)$ (times the Fermi function) even deep below the Fermi energy with high accuracy (see, e.g., Ref. [6]). Therefore it is desirable to understand the origin of resonances given by (19), even if these excitations are not as coherent as low-energy excitations in a Landau Fermi liquid.

Hubbard bands and the Mott transition

Let us consider the atomic limit of the Hubbard model, i.e., no hopping, $t_{ij} = 0$. The Green function then becomes momentum-independent and reads

$$G^{\mathrm{at}}_{\boldsymbol{k}\sigma}(\omega) = \frac{n_{-\sigma}}{\omega + \mu - U} + \frac{1 - n_{-\sigma}}{\omega + \mu}\,, \tag{22}$$

which corresponds to a spectral function with two δ peaks separated by an energy U, and for half-filling the system is *insulating*. What happens now if we turn on the hopping t_{ij}? The δ peaks in the spectral function will broaden so that two subbands develop, the *Hubbard bands*. Note that these subbands are not one-electron bands as in non-interacting systems. For example, the upper Hubbard band describes the spectrum of charge excitations on top of the filled lower Hubbard band. If the hopping is increased further, or the Hubbard interaction U decreased, these Hubbard bands will eventually overlap and the system will become metallic at a critical value U_c on the order of the bandwidth. This correlation-induced *metal-insulator transition* does not break translational invariance and is called the Mott transition, as it was originally put forward by Mott [7].

Starting from the atomic limit, the simplest and rather crude method to capture the Mott phenomenon is the so-called Hubbard-I approximation: one obtains the atomic self-energy from (22) and uses it in the Dyson equation. However, this ad-hoc approximation leads to several undesirable pathologies (see Ref. [8] for a discussion). Starting from the weak-coupling side, a reasonable picture of the Mott transition can be provided by, e.g., the Gutzwiller wave function (see [9] for a review); however, there are also some shortcomings in this and other variational approaches. In fact, one of the successes of DMFT is its description of the Mott transition; in Sec. 4 we will mention some of these results.

2 Fermions in infinite dimensions

Historically, DMFT began with the discovery of simplifications that occur in the limit of infinite spatial dimensions [10], which we will now discuss. First of all, it is of course straightforward

to generalize the three-dimensional simple cubic lattice to the d-dimensional hypercubic lattice. The hypercubic lattice has the unit cell basis vectors

$$\boldsymbol{e}_1 = (1, 0, 0, \ldots, 0)\,, \tag{23}$$

$$\boldsymbol{e}_2 = (0, 1, 0, \ldots, 0)\,, \tag{24}$$

$$\ldots \tag{25}$$

$$\boldsymbol{e}_d = (0, 0, 0, \ldots, 1)\,. \tag{26}$$

A nearest-neighbor hopping amplitude t_{ij} and corresponding dispersion then have the form

$$t_{ij} = t(\boldsymbol{R}_i - \boldsymbol{R}_j) = \begin{cases} -t & \text{if } \boldsymbol{R}_i - \boldsymbol{R}_j = \pm \boldsymbol{e}_n \\ 0 & \text{otherwise} \end{cases}, \qquad \epsilon_{\boldsymbol{k}} = -2t \sum_{i=1}^{d} \cos k_i\,. \tag{27}$$

We now consider the limit $d \to \infty$ and obtain the limit of the density of states (11), in two ways. The first and rather elegant way proceeds by appealing to the central limit theorem of probability theory [10]. For this, consider the random variables $X_i = \sqrt{2}\cos k_i$, with the independent random variables k_i each distributed uniformly in $[-\pi : \pi]$. X_i has zero mean and unit variance, $\int_{-\pi}^{\pi} \frac{dk_i}{2\pi} X_i^2 = 1$. By the central limit theorem, for $d \to \infty$ the random variable $X_d = \frac{1}{\sqrt{d}} \sum_{i=1}^{d} X_i$ *converges in law* to a normal distributed random variable X with zero mean and unit variance. This means that the distribution function of X_d converges to the normal distribution $f(x) = \exp(-x^2/2)/\sqrt{2\pi}$. Next the density of states $\rho(\epsilon)$ can be regarded as the distribution function of the random variable $\sqrt{2d}\, t\, X_d$. We conclude that a finite density of states is obtained for $d \to \infty$ if the hopping amplitude is scaled proportional to $d^{-1/2}$,

$$\rho(\epsilon) = \int \frac{d^d k}{(2\pi)^d}\, \delta(\epsilon - \epsilon_{\boldsymbol{k}}) \tag{28a}$$

$$= \frac{1}{2\pi |t_*|}\, \exp\left[-\frac{\epsilon^2}{2t_*^2}\right] \qquad \text{for } t = \frac{t_*}{\sqrt{2d}}\,, \tag{28b}$$

with t_* independent of d. Hence nearest-neighbor hopping on the hypercubic lattice, if scaled appropriately, leads to a Gaussian density of states. In Fig. 1, which shows the density of states for hopping on hypercubic lattice for several d, the trend towards the Gaussian density of states for large d can be recognized.

The second way to obtain this density of states uses the Fourier transform of $\rho(\epsilon)$ [12], which factorizes:

$$\Phi(s) = \int_{-\infty}^{\infty} d\epsilon\; e^{is\epsilon}\; \rho(\epsilon) = \int \frac{d^d k}{(2\pi)^d}\; e^{is\epsilon_{\boldsymbol{k}}} \tag{29}$$

$$= \left[\int_{-\pi}^{\pi} \frac{dk}{2\pi}\; \exp\left(-\frac{2ist_*}{\sqrt{2d}}\; \cos k\right)\right]^d = J_0\left(\frac{2t_*}{\sqrt{2d}}\right)^d \tag{30}$$

$$= \left[1 - \frac{t_*^2 s^2}{2d} + O\left(\frac{1}{d^2}\right)\right]^d = \exp\left[-\frac{t_*^2 s^2}{2} + O\left(\frac{1}{d}\right)\right]\,, \tag{31}$$

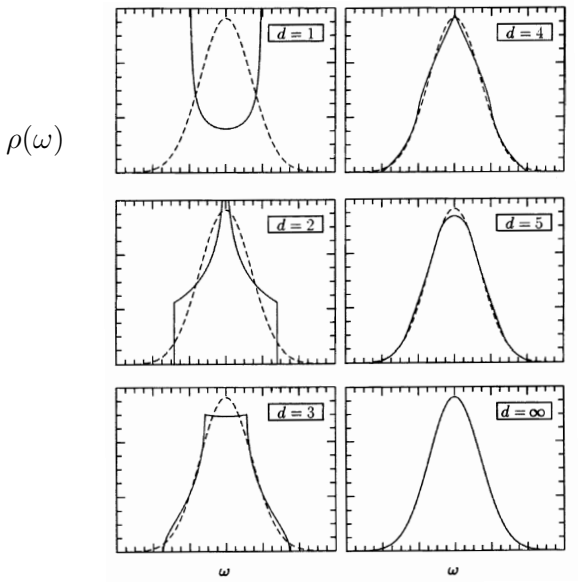

Fig. 1: *Density of states for hopping on hypercubic lattice for several d, compared to the Gaussian that is obtained in $d \to \infty$. From Ref. [2].*

where $J_0(z)$ is a Bessel function. The inverse transform is then

$$\rho(\epsilon) = \int_{-\infty}^{\infty} \frac{d\epsilon}{2\pi}\, e^{-is\epsilon}\, \Phi(s) = \frac{1}{2\pi|t_*|}\, \exp\left[-\frac{\epsilon^2}{2t_*^2} + O\left(\frac{1}{d}\right)\right] . \tag{32}$$

In fact, this calculation is similar to the proof ideas behind the central limit theorem, for which Fourier transforms of probability function are also used.

The important conclusion from these considerations is that the nearest-neighbor hopping amplitude must be scaled with $1/\sqrt{d}$ to obtain a meaningful finite limit. This statement can be generalized as follows: each hopping amplitude t_n must be scaled proportional to $1/\sqrt{Z_n}$, where Z_n is the number of sites that are connected by t_n, e.g., $Z_1 = 2d$ for nearest-neighbor hopping and $Z_2 = (2d-1)2d = (Z-1)Z$ for next-nearest-neighbor hopping on the hypercubic lattice, and so on.

Note that the density of states extends up to infinite positive and negative energies ϵ, even after the scaling (28). An infinite bandwidth results also for other generalized lattices, such as the face-centered-hypercubic lattice [11] (which is asymmetric and has one finite band edge) or the hyperdiamond lattice [13] (for which the symmetric density of states vanishes at $\epsilon = 0$). One of the few lattices with finite bandwidth is the Bethe lattice, i.e., an infinite Cayley tree of which each node has Z nearest neighbors. This recursively defined lattice (which is not a crystal lattice) has a semi-elliptic density of states with a finite bandwidth in the limit $Z \to \infty$ for scaled nearest-neighbor hopping $t = t_*/\sqrt{Z}$,

$$\rho_{\text{Bethe}}(\epsilon) = \begin{cases} \dfrac{\sqrt{4t_*^2 - \epsilon^2}}{2\pi t_*^2} & \text{for } |\epsilon| \le 2|t_*| \\ 0 & \text{otherwise} \end{cases} . \tag{33}$$

This result is best obtained with recursive methods and can be generalized to next-nearest-neighbor and longer-range hopping (see Refs. [14,15] and references therein).

The infinite band edges for nearest-neighbor hopping on regular lattice may seem problematic at first glance. After all we are interested in using the infinite-dimensional limit as an approximation to finite-dimensional lattices, for which finite hopping amplitude always imply finite band edges. The practical solution is to use the simplifications that result from the infinite-dimensional limit (see the following sections) and to plug in the non-interacting density of states of the system of interest everywhere. Some justification for this scheme comes from two observations: (i) In infinite dimensions the dispersion $\epsilon_{\boldsymbol{k}}$ typically enters only via the density of states (at least into single-particle quantities), so that the detailed lattice structure does not enter. (ii) For any single-band density of states one can always construct a corresponding set of hopping amplitudes (both for the infinite-dimensional hypercubic [16] and Bethe lattice [14]); in particular, densities of states with finite bandwidth are perfectly possible, although they usually require long-range hopping.

3 Simplifications for many-body theory

We now turn to the consequences that the limit $d \to \infty$ has for many-body theory [12, 17], in particular for the self-energy (defined in 13). This is best discussed in terms of Feynman diagrams for Green functions [4,5], of which we first review some basics.

A guide to Feynman diagrams

Feynman diagrams for single-particle Green functions (for arbitrary quadratic H_0 and two-particle interaction H_1) are built from the following elements:

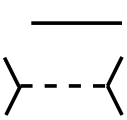
= non-interacting Green function line $\boldsymbol{G}^{(0)}$, (34)

= interaction vertex, (35)


= full (interacting) Green function line $\boldsymbol{G}$. (36)

The perturbation expansion in H_1 then yields the following series of diagrams (unlabeled, and arrows omitted) for the Green function:

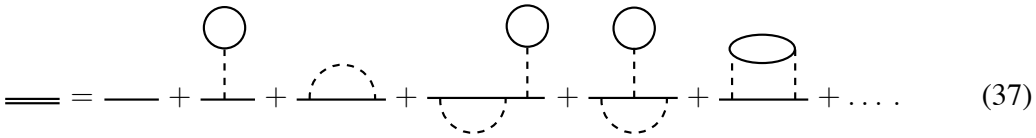
(37)

Clearly some parts of the diagram occur repeatedly. Therefore one defines proper self-energy diagrams, which are “one-particle irreducible” (i.e., cannot be cut in two pieces by cutting a

single solid line) and have their external vertices amputated. Here are some examples:

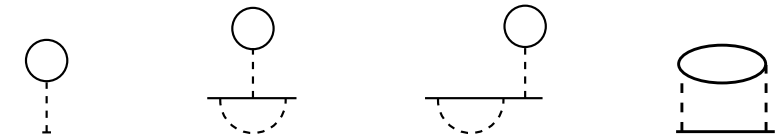

. (38)

proper proper not proper proper (39)

From these diagrams one builds the self-energy,

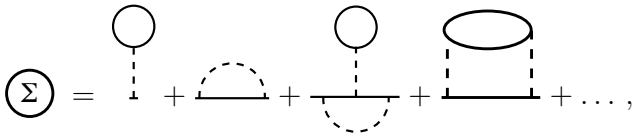

(40)

which, when combined with (14), indeed yields (36). So far we have considered an expansion of the form $\boldsymbol{\Sigma}[\boldsymbol{G}^{(0)}]$,[3] i.e., in terms of the free Green function $\boldsymbol{G}^{(0)}$. These diagrams still contain self-energy insertions in their internal lines. The next step is therefore to construct the *skeleton expansion* which instead uses full (interacting) Green function lines:

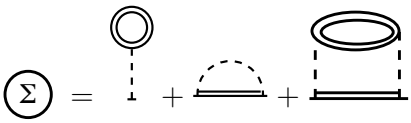

(41)

Clearly one must be careful not to include diagrams more than once, especially in higher orders. The skeleton expansion $\boldsymbol{\Sigma}[\boldsymbol{G}]$ is a useful representation to analyze the self-energy in the limit $d \to \infty$.

Power counting in $1/d$

We now study first the d dependence of $G_{ij\sigma}(\omega)$ in the limit $d \to \infty$, for scaled hopping amplitudes,

$$t_{ij} = t^*_{ij}\, d^{-\frac{1}{2}||\boldsymbol{R}_i - \boldsymbol{R}_j||}\,. \tag{42}$$

Here $||\boldsymbol{R}_i - \boldsymbol{R}_j||$ is the shortest number of lattice steps from $\boldsymbol{R}_i$ to $\boldsymbol{R}_j$ on the hypercubic lattice, and hence proportional to the number of sites connected by the hopping amplitude t_{ij}, so that (42) has the correct scaling. By our construction the kinetic energy is finite in the limit $d \to \infty$, which can be expressed in terms of the Green function,

$$E_{\text{kin},\sigma} = \sum_{ij} t_{ij} \langle c^+_{i\sigma} c_{j\sigma} \rangle = \sum_{ij} t_{ij} \int_{-\infty}^{\infty} \frac{d\omega}{2\pi i}\, G_{ij\sigma}(\omega)\, e^{i\omega 0^+} = O(d^0)\,. \tag{43}$$

Here the double sum yields a contribution of order $Ld^{||\boldsymbol{R}_i - \boldsymbol{R}_j||}$. Hence we can conclude

$$G_{ij\sigma}(\omega) = O(d^{-\frac{1}{2}||\boldsymbol{R}_i - \boldsymbol{R}_j||})\,, \qquad\qquad G_{ii\sigma}(\omega) = O(d^0)\,, \tag{44}$$

i.e., the Green function decays rapidly with distance, which leads to simplifications for the Feynman diagrams.

[3] This is of course a functional dependence of $\boldsymbol{\Sigma}$ on $\boldsymbol{G}^{(0)}$, because the whole matrix $\boldsymbol{G}^{(0)}(i\omega_n)$ and also the frequency dependence enter into the value of the Feynman diagrams due to summations over internal lines.

Local self-energy

We know analyze the consequences for the self-energy. For this discussion, however, we work with Hugenholtz diagrams instead, which combine direct and exchange diagrams into a box vertex [5]. However, for the Hubbard interaction here are no exchange diagrams anyway. We thus make the replacement

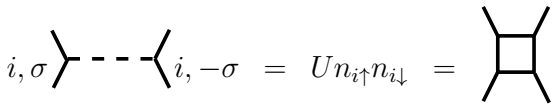

(45)

In terms of these diagrams, the skeleton expansion takes the form

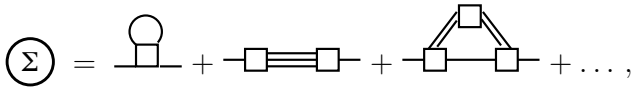

(46)

and has the property that by construction any two vertices are joined through Green function lines via at least three independent paths. Namely, suppose there is only one such path; then the diagram is one-particle irreducible, a contradiction. If there are only two paths, then they must run through a diagram part which is a self-energy insertion, which is also a contradiction.
Now consider an arbitrary diagram (in position space, so that the interaction vertices are labeled by lattice site vectors), in which two internal vertices labeled by i and j appear,

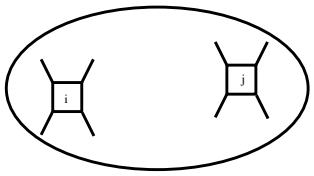

(47)

Let us hold i fixed for the moment. We now compare the case $j \neq i$ with the case $j = i$. Suppose $j \neq i$. As discussed above, there are three independent paths from the vertex i to the vertex j. The Green function lines on these paths can thus contribute at most $O(d^{-\frac{3}{2}||\boldsymbol{R}_i - \boldsymbol{R}_j||})$ (for example, less if there is another intermediate site $\boldsymbol{R}_k$ on a path). The summation over j will then yield an order $O(d^{||\boldsymbol{R}_i - \boldsymbol{R}_j||})$. As a consequence, any skeleton diagram is suppressed at least by a factor $O(d^{-\frac{1}{2}||\boldsymbol{R}_i - \boldsymbol{R}_j||})$, for example this one:

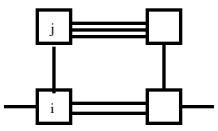

(48)

By contrast, for $j = i$ the Green functions are of order $O(d^0)$, and there is no summation. We thus conclude that only the case $i = j$ contributes in the limit $d \to \infty$, i.e., all diagrams in the skeleton expansion $\boldsymbol{\Sigma}[\boldsymbol{G}]$ have the same lattice site label at all their internal and external vertices. Hence the self-energy is site-diagonal ("local"),

$$\Sigma_{ij\sigma}(\omega) = \delta_{ij} \; \Sigma_{ii\sigma}(\omega) = \delta_{ij} \; \Sigma_{\sigma}(\omega) \, , \tag{49}$$

or, equivalently, momentum-independent in $\boldsymbol{k}$ space,

$$\Sigma_{\boldsymbol{k}\sigma}(\omega) = \Sigma_\sigma(\omega)\,. \tag{50}$$

Furthermore, *the self-energy $\Sigma_\sigma(\omega)$ is a functional only of the local Green function $G_\sigma(\omega)$*, because all internal vertices in the skeleton expansion have the same site label.
The simple form of the self-energy has some immediate consequences also for the Green function (13), namely

$$G_{\boldsymbol{k}\sigma}(\omega) = \frac{1}{\omega + \mu - \epsilon_{\boldsymbol{k}} - \Sigma_\sigma(\omega)} = G^{(0)}_{\boldsymbol{k}\sigma}(\omega - \Sigma_\sigma(\omega))\,, \tag{51}$$

and in particular the local Green function becomes

$$G_\sigma(\omega) = \int \frac{d^dk}{(2\pi)^d} \frac{1}{\omega + \mu - \epsilon_{\boldsymbol{k}} - \Sigma_\sigma(\omega)} \tag{52}$$

$$= \int_{-\infty}^{\infty} d\omega\, \frac{\rho(\epsilon)}{\omega + \mu - \Sigma_\sigma(\omega) - \epsilon}\,. \tag{53}$$

The last equation thus provides a relation between the local self-energy and the local Green function, and depends only on the dispersion via the free density of states. We will come back to this relation in the next section.

4 Dynamical mean-field theory

In the last section we have seen that the self-energy becomes site-diagonal and momentum-independent in the limit $d \to \infty$. The last step is now to actually construct the functional $\Sigma_\sigma[G_\sigma]$ [1–3,18,19], which will complete the derivation of the DMFT equations.

Mapping onto effective impurity models

Consider a single-site action, $\mathcal{A} = \mathcal{A}_1 + \mathcal{A}_2$, consisting of a quadratic part and an interaction,

$$\mathcal{A}_1 = \int_0^\beta d\tau \int_0^\beta d\tau' \sum_\sigma c^*_\sigma(\tau)\, \mathcal{G}^{-1}_\sigma(\tau,\tau')\, c_\sigma(\tau') = \sum_{n,\sigma} c^*_\sigma(i\omega_n)\, \mathcal{G}_\sigma(i\omega_n)^{-1}\, c_\sigma(i\omega_n), \tag{54a}$$

$$\mathcal{A}_2 = -U \int_0^\beta d\tau\; c^*_\uparrow(\tau) c_\uparrow(\tau) c^*_\downarrow(\tau) c_\downarrow(\tau), \tag{54b}$$

with some as yet unfixed "free" Green function $(\boldsymbol{\mathcal{G}}^{-1})_{\tau,\tau'} = \mathcal{G}^{-1}_\sigma(\tau,\tau')$, which also depends only on imaginary-time differences. The goal is now to match this action to that of Hubbard model in infinite dimensions.

Suppose that we calculate the imaginary-time-ordered Green function of the single degree of freedom c from the action (54), and Fourier transform to Matsubara frequencies. This is abbreviated as

$$G_\sigma(i\omega_n) = \langle c_\sigma(i\omega_n) c^*_\sigma(i\omega_n) \rangle_{\mathcal{A}[\boldsymbol{\mathcal{G}}]} \,. \tag{55}$$

Then define the impurity *impurity self-energy* $\widetilde{\boldsymbol{\Sigma}}$ via the *impurity Dyson equation*,

$$\boldsymbol{G} = \left[\boldsymbol{\mathcal{G}}^{-1} - \widetilde{\boldsymbol{\Sigma}} \right]^{-1} . \tag{56}$$

Now consider the diagrams in the skeleton expansion of $\widetilde{\boldsymbol{\Sigma}}[\boldsymbol{G}]$,

$\widetilde{\boldsymbol{\Sigma}}[\boldsymbol{G}] \;=$ 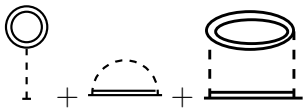 $+ \ldots ,$ (57)

in which of course only the single site of (54) occurs. However, since the local Hubbard interaction is the same both for the lattice Hubbard model and the single-site action, this skeleton expansion is exactly the same as that for the Hubbard model (41), i.e.,

$$\widetilde{\boldsymbol{\Sigma}}[\boldsymbol{G}] = \boldsymbol{\Sigma}[\boldsymbol{G}] \,. \tag{58}$$

This shows that the desired functional $\Sigma_\sigma[G_\sigma]$ can be obtained by solving the single-site problem (54).

Dynamical mean-field equations

We summarize again the three DMFT equations, which determine three unknowns: the local Green function $G_\sigma(i\omega_n)$, the *dynamical mean field* (or *Weiss field*) $\mathcal{G}_\sigma(i\omega_n)$, and the local self-energy $\Sigma_\sigma(i\omega_n)$:

$$G_\sigma(i\omega_n) = \langle c_\sigma(i\omega_n) c^*_\sigma(i\omega_n) \rangle_{\mathcal{A}[\mathcal{G}]}, \tag{DMFT-1}$$

$$G_\sigma(i\omega_n) = \left[\mathcal{G}_\sigma(i\omega_n)^{-1} - \Sigma_\sigma(i\omega_n) \right]^{-1}, \tag{DMFT-2}$$

$$G_\sigma(i\omega_n) = \int d\epsilon \, \frac{\rho(\epsilon)}{i\omega_n + \mu - \Sigma_\sigma(i\omega_n) - \epsilon}. \tag{DMFT-3}$$

Note that the self-consistency equation (53) provides precisely the needed relation (DMFT-3) to fix the Weiss field $\mathcal{G}_\sigma$. After all, it must be ensured that one solves the correct single-site problem, i.e., the one which indeed corresponds to the Hubbard model on a lattice with density of states $\rho(\epsilon)$.

A typical iterative solution then proceeds a follows. Start with some Weiss field $\mathcal{G}_\sigma$, obtain G_σ from (DMFT-1), determine Σ_σ from the impurity Dyson equation (DMFT-2), calculate G_σ from self-consistency equation (DMFT-3), obtain $\mathcal{G}_\sigma$ by using (DMFT-2) again, and repeat until convergence is reached.

Of course the DMFT equations should produce the correct noninteracting and atomic limits. (i) In the noninteracting case we have $U = 0$ and thus $\Sigma_\sigma(i\omega_n) = 0$. Furthermore it follows from (DMFT-3) that then $G_\sigma(i\omega_n) = G^{(0)}_\sigma(i\omega_n)$. Finally (DMFT-2) gives $\mathcal{G}_\sigma(i\omega_n) = G_\sigma(i\omega_n)$, and this agrees with (DMFT-1) for $U = 0$. (ii) On the other hand, in the atomic limit we have $t_{ij} = 0$ and $\epsilon_{\boldsymbol{k}} = 0$, i.e., $\rho(\epsilon) = \delta(\epsilon)$. From (DMFT-3) we obtain $G_\sigma(i\omega_n) = [i\omega_n + \mu - \Sigma_\sigma(i\omega_n)]^{-1}$, and (DMFT-2) yields $\mathcal{G}_\sigma(i\omega_n)^{-1} = i\omega_n + \mu$, i.e., $\mathcal{G}^{-1}_\sigma(\tau) = -\partial_\tau + \mu$, which agrees with (DMFT-1) for $t_{ij} = 0$.

For general interaction U, the local action (54) clearly represents the most difficult of the DMFT equations. To obtain the impurity Green function from it, a dynamical single-site problem must be solved, usually with numerical methods. For finite temperatures quantum and thermal averages can be stochastically sample with quantum Monte Carlo (QMC) methods, such as the Hirsch-Fye QMC algorithm [19–21, 1] and continuous-time (CT) QMC [22–24]. Methods that also work for zero temperature include exact diagonalization (ED) [25–27], the numerical renormalization group (NRG) [28, 29] and the density-matrix renormalization group (DMRG) [30]. A number of perturbative or semianalytic methods is also available.

To use these "impurity solvers", the single-site action (54) is not used directly, but rather an impurity problem defined by a Hamiltonian is considered, usually by constructing a single-impurity Anderson model (SIAM):

$$H_{\text{SIAM}} = \sum_{\ell\sigma} \epsilon_\ell \, a^+_{\ell\sigma} a_{\ell\sigma} + \sum_{\ell\sigma} V_\ell \, (a^+_{\ell\sigma} c_\sigma + c^+_\sigma a_{\ell\sigma}) + U c^+_\uparrow c_\uparrow \, c^+_\downarrow c_\downarrow \, . \tag{59}$$

Here the fermions $a_{\ell\sigma}$ represent a non-interacting bath which hosts the interacting fermion c_σ. This bath can be at once integrated out from the action which represents H_{SIAM}, because this involves only Gaussian integrals. The resulting action is then precisely of the form (54), with

$$\mathcal{G}^{-1}_\sigma(i\omega_n) = i\omega_n + \mu - \frac{1}{\pi} \int\limits_{-\infty}^{\infty} d\omega \frac{\Delta(\omega)}{i\omega_n - \omega} \, , \qquad \Delta(\omega) = \pi \sum_\ell V^2_\ell \delta(\omega - \epsilon_\ell) \, , \tag{60}$$

where $\Delta(\omega)$ is called the hybridization function. In the DMFT cycle one must now find the parameters V_ℓ and ϵ_ℓ that allow a self-consistent DMFT solution. Then one has found the appropriate SIAM that represents the Hubbard model in DMFT.

For reference we note that the self-consistency equation (DMFT-3) yields a simple relation for next-neighbor hopping t_* on the Bethe lattice with density of states (33),

$$\mathcal{G}_\sigma(i\omega_n) = i\omega_n + \mu - t^2_* G(i\omega_n) \, . \tag{61}$$

This relation and generalizations for other types of hopping are discussed in Refs. [1,16,14,15].

Results for the Hubbard model

Some aspects of the spectrum and DMFT phase diagram of the Hubbard model were discussed already in the Lecture of D. Vollhardt. Fig. 2 shows the zero-temperature spectral function for

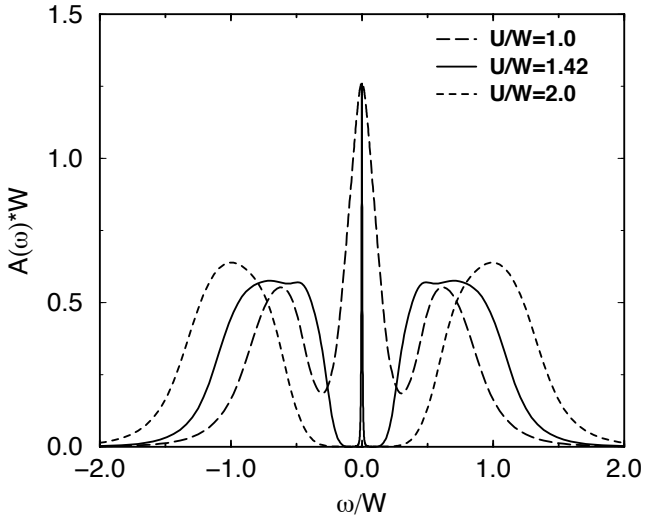

Fig. 2: *Zero-temperature spectral function for the homogeneous phase of the Hubbard model on the Bethe lattice with nearest-neighbor hopping and bandwidth $W = 4|t_*|$ at half-filling, evaluated with NRG. From Ref. [28].*

the homogeneous phase of the Hubbard model on the Bethe lattice with nearest-neighbor hopping and bandwidth $W = 4|t_*|$ at half-filling, evaluated with NRG. Three values of U are shown, one in the metallic phase (three peaks in the spectral function), one close to the critical value U_c, and one for the insulating phase (with gap in the spectral function). At the Fermi energy the spectral function has the same value for all U in the metallic phase; this is a consequence of Luttinger's theorem [12]. In the metallic phase the weight of the central peak is proportional to the Fermi liquid quasiparticle renormalization factor Z (see (21)), whereas the outer two peaks are the developing Hubbard bands.

Fig. 3 shows the renormalization factor Z obtained with various methods. It starts from $Z = 1$ for the non-interacting case and decreases as U is increased, corresponding to the decreasing width of the central peak in the spectral function and an increasingly flatter dispersion. At U_c, the half-filled system becomes localized and Z vanishes accordingly.

The Falicov-Kimball model, a solvable example

The Falicov-Kimball model is a simplified version of the Hubbard model, in which only one of the two spin species is mobile (relabeled as d_i), while the other (relabeled as f_i) is not. For this model the Green function can be obtained explicitly from the DMFT action [31]. The Hamiltonian reads

$$H = \sum_{ij} t_{ij}\, d_i^+ d_j \; + E_f \sum_i f_i^+ f_i \; + U \sum_i d_i^+ d_i \; f_i^+ f_i \;\; , \tag{62}$$

i.e. the d electrons are moving in front of a background of static f electrons, whose configuration is chosen such that it optimizes the free energy. In principle this makes the model quite complicated, as one needs the spectrum of H for all the possible f configurations. In dimensions $d \geq 2$ it is known that at half-filling on a bipartite lattice checkerboard order of the f

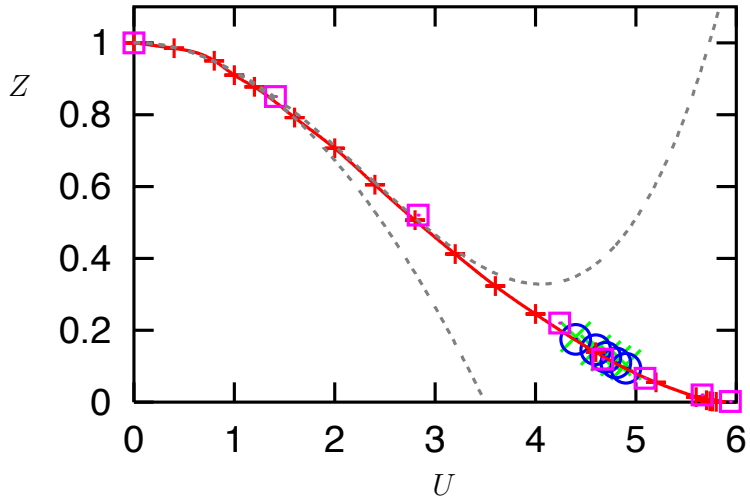

Fig. 3: *Quasiparticle weight Z for the half-filled Hubbard model on the Bethe lattice (with $t_* = 1$) in DMFT. Crosses $+$: NRG; squares: ED; crosses $\times$ and circles: QMC extrapolations; lower dashed line: 2nd order perturbation theory in U, upper dashed line: 4th order perturbation theory in U. From Ref. [16].*

electrons appears in the ground state and persists up to a finite critical temperature [32]. Here we consider only the homogeneous phase in DMFT for simplicity.

Since there is no hopping amplitude for the f electrons, the DMFT self-consistency yields at once $\mathcal{G}_f^{-1} = -\partial_\tau + \mu + E_f$, as explained above for the atomic limit. The DMFT action is thus given by

$$\mathcal{A} = \int_0^\beta d\tau \int_0^\beta d\tau' d^*(\tau)\, \mathcal{G}_d^{-1}(\tau,\tau')\, d(\tau') + \int_0^\beta d\tau f^*(\tau)(\partial_\tau - \mu + E_f)\, f(\tau) - U \int_0^\beta d\tau\; d^*(\tau)d(\tau)f^*(\tau)f(\tau). \tag{63}$$

Now the f electrons can be integrated out at each lattice site, i.e., they are in the atomic limit (cf. Sec. 1). This leads to

$$G_d(i\omega_n) = \langle d(i\omega_n)d^*(i\omega_n)\rangle_{\mathcal{A}} = \frac{n_f}{\mathcal{G}_d(i\omega_n)^{-1} - U} + \frac{1-n_f}{\mathcal{G}_d(i\omega_n)^{-1}}\,, \tag{64}$$

which must be solved together with the other two DMFT equations

$$G_d(i\omega_n) = \int_{-\infty}^{\infty} \frac{d\epsilon\; \rho_d(\epsilon)}{i\omega_n + \mu - \Sigma_d(i\omega_n) - \epsilon}\,, \tag{65}$$

$$G_d(i\omega_n)^{-1} = \mathcal{G}_d(i\omega_n)^{-1} - \Sigma_d(i\omega_n)\,. \tag{66}$$

This set of equations determines the d-electron Green function $G_d(i\omega_n)$ for any density of states $\rho_d(\epsilon)$. Analytically continuation to real frequencies shows at once that the spectra in the homogeneous phase are independent of temperature (but this no longer holds in the checkerboard

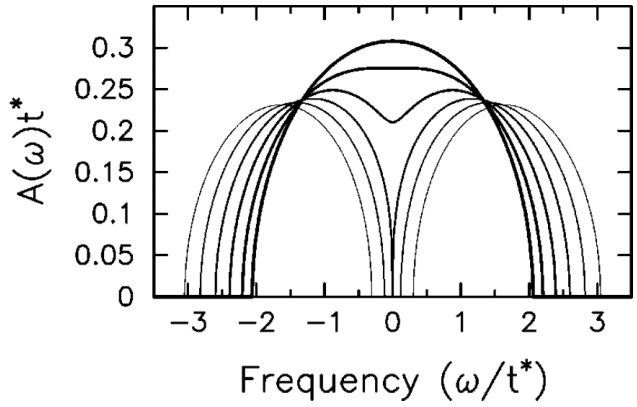

Fig. 4: *Spectral function of itinerant d electrons for the Falicov-Kimball model in DMFT for nearest-neighbor hopping on the Bethe lattice, homogeneous phase, $n_d = n_f = \frac{1}{2}$, $U = 0.5,\ 1.0,\ \ldots\ 3.0$. From Ref. [31].*

phase). Fig. 4 shows the spectral function $A_d(\omega)$ for several U for the Bethe lattice (with nearest-neighbor hopping $t_* = 1$). In particular there is a Mott metal-insulator transition taking place at $U_c = 2$; for larger U, a band gap develops. Nevertheless, the transition is qualitatively different from that in the Hubbard model. For example, for the Falicov-Kimball model it can be shown that from the low-energy form of the self-energy that for $0 < U < U_c$ the metallic state is not a Landau Fermi liquid; as a consequence, the spectral function is not pinned at the Fermi surface.

It is also possible to solve for d self-energy as a functional of the d Green function, i.e., for the skeleton functional[4] $\Sigma_d[G_d]$ [8]

$$\Sigma_d(i\omega_n) = \frac{U}{2} - \frac{1}{2G_d(i\omega_n)} \pm \sqrt{\left(\frac{U}{2} - \frac{1}{2G_d(i\omega_n)}\right)^2 + \frac{Un_f}{G_d(i\omega_n)}}\,. \tag{67}$$

Just like any skeleton expansion, this relation holds for any density of state $\rho(\epsilon)$.

5 Summary and outlook

The goal of this lecture was to demonstrate the origin of DMFT, i.e., to show how the infinite-dimensional Hubbard model can be mapped onto a dynamical single-site problem in an effective bath, which has to be determined self-consistently. In the other lectures several further aspects of DMFT will be discussed. For one, some of the numerical approaches that were only mentioned in this lecture will be explained in detail. Second, DMFT will be combined with ab-initio band structure methods to make quantitative predictions about correlated materials. Finally, several extensions of DMFT to correlated clusters (instead of a single correlated site) will be developed, which improve the description for finite-dimensional systems.

[4] Note that in the DMFT solution for the Falicov-Kimball model this functional is in fact a function: $\Sigma_d(i\omega_n)$ depends only on $G_d(i\omega_n)$ at the same frequency. This is certainly not the case for the Hubbard model.

Acknowledgment

Support of the Deutsche Forschungsgemeinschaft through FOR1346 is gratefully acknowledged.

References

[1] A. Georges, G. Kotliar, W. Krauth, and M. J. Rozenberg, Rev. Mod. Phys. **68**, 13 (1996)

[2] D. Vollhardt, in *Correlated Electron Systems*, edited by V. J. Emery (World Scientific, Singapore, 1993) p. 57

[3] D. Vollhardt, in *Lectures on the Physics of Strongly Correlated Systems XIV*, *AIP Conference Proceedings*, vol. 1297, ed. by A. Avella, F. Mancini (American Institute of Physics, Melville, 2010), p. 339; arXiv:1004.5069

[4] A. L. Fetter and J. D. Walecka, *Quantum Theory of Many-Particle Systems* (McGraw-Hill, 1971)

[5] J. W. Negele and H. Orland, *Quantum Many-Particle Systems* (Addison-Wesley, 1988)

[6] X. J. Zhou, T. Cuk, T. Devereaux, N. Nagaosa, and Z.-X. Shen, in: J. R. Schrieffer (ed.), *Handbook of High-Temperature Superconductivity: Theory and Experiment* (Springer, 2007), p. 87; arXiv:cond-mat/0604284

[7] N. F. Mott, Proc. Phys. Soc. A **62**, 416 (1947)

[8] F. Gebhard, *The Mott Metal-Insulator Transition* (Springer, Berlin, 1997)

[9] D. Vollhardt, Rev. Mod. Phys. **56**, 99 (1984)

[10] W. Metzner and D. Vollhardt, Phys. Rev. Lett. **62**, 324 (1989)

[11] E. Müller-Hartmann, in: E. Talik and J. Szade (eds.), *Proceedings of the V. Symposium "Physics of Metals"* (Ustroń, 1991)

[12] E. Müller-Hartmann, Z. Phys. B **74**, 507 (1989)

[13] G. Santoro, M. Airoldi, S. Sorella, and E. Tosatti, Phys. Rev. B **47**, 16216 (1993)

[14] M. Eckstein, M. Kollar, K. Byczuk and D. Vollhardt, Phys. Rev. B **71**, 235119 (2005)

[15] M. Kollar, M. Eckstein, K. Byczuk, N. Blümer, P. van Dongen, M. H. Radke de Cuba, W. Metzner, D. Tanaskovic, V. Dobrosavljevic, G. Kotliar, and D. Vollhardt, Ann. Phys. (Leipzig) **14**, 642 (2005)

[16] N. Blümer, *Metal-Insulator Transition and Optical Conductivity in High Dimensions* (Shaker Verlag, Aachen, 2003)

[17] E. Müller-Hartmann, Z. Phys. B **76**, 211 (1989)

[18] A. Georges and G. Kotliar, Phys. Rev. B **45**, 6479 (1992)

[19] M. Jarrell, Phys. Rev. Lett. **69**, 168 (1992)

[20] M. J. Rozenberg, X. Y. Zhang, and G. Kotliar, Phys. Rev. Lett. **69**, 1236 (1992)

[21] A. Georges and W. Krauth, Phys. Rev. Lett. **69**, 1240 (1992)

[22] A. N. Rubtsov, V. V. Savkin, and A. I. Lichtenstein, Phys. Rev. B **72**, 035122 (2005)

[23] P. Werner, A. Comanac, L. de' Medici, M. Troyer, and A. J. Millis, Phys. Rev. Lett. **97**, 076405 (2006)

[24] K. Haule, Phys. Rev. B **75**, 155113 (2007)

[25] M. Caffarel and W. Krauth, Phys. Rev. Lett. **72**, 1545 (1994)

[26] Q. Si, M. J. Rozenberg, G. Kotliar, and A. E. Ruckenstein, Phys. Rev. Lett. **72**, 2761 (1994)

[27] M. J. Rozenberg, G. Moeller, and G. Kotliar, Mod. Phys. Lett. B **8**, 535 (1994)

[28] R. Bulla, Phys. Rev. Lett. **83**, 136 (1999)

[29] R. Bulla, T. A. Costi, and Th. Pruschke, Rev. Mod. Phys. **80**, 395 (2008)

[30] M. Karski, C. Raas, and G. S. Uhrig, Phys. Rev. B **77**, 075116 (2008)

[31] J. K. Freericks and V. Zlatić, Rev. Mod. Phys. **75**, 1333 (2003)

[32] T. Kennedy and E. H. Lieb, Physica A **138** 320 (1986)